HHS Public Access

Author manuscript

Kidney Int. Author manuscript; available in PMC 2021 March 01.

Published in final edited form as:

Kidney Int. 2020 March ; 97(3): 567–579. doi:10.1016/j.kint.2019.09.026.

Whole exome sequencing identified *ATP6V1C2* as a novel candidate gene for recessive distal renal tubular acidosis

Tilman Jobst-Schwan[1,¶], **Verena Klämbt**[1,¶], **Maureen Tarsio**[2], **John F. Heneghan**[3], **Amar J. Majmundar**[1], **Shirlee Shril**[1], **Florian Buerger**[1], **Isabel Ottlewski**[1], **Boris E. Shmukler**[3], **Rezan Topaloglu**[4], **Seema Hashmi**[5], **Farkhanda Hafeez**[6], **Francesco Emma**[7], **Marcella Greco**[7], **Guido F. Laube**[8], **Hanan M. Fathy**[9], **Martin Pohl**[10], **Jutta Gellermann**[11], **Danko Milosevic**[12], **Michelle A. Baum**[1], **Shrikant Mane**[13,14], **Richard P. Lifton**[13,14], **Patricia M. Kane**[2], **Seth Alper**[3], **Friedhelm Hildebrandt**[1]

[1]Division of Nephrology, Department of Pediatrics, Boston Children's Hospital, Harvard Medical School, Boston, Massachusetts, USA [2]Department of Biochemistry and Molecular Biology, SUNY Upstate Medical University, Syracuse, NY [3]Division of Nephrology, Department of Medicine, Beth Israel Deaconess Medical Center, Harvard Medical School, Boston, Massachusetts, USA [4]Department of Pediatric Nephrology, Hacettepe University Faculty of Medicine, Ankara Turkey [5]Department of Pediatric Nephrology, Sindh Institute of Urology and Transplantation, Karachi, Pakistan [6]Department of Pediatric Nephrology, The Children's Hospital and Institute of Child Health, Lahore [7]Department of Pediatric Subspecialties, Bambino Gesù Children's Hospital - IRCCS, Rome, Italy [8]Nephrology Unit, „University Children's Hospital Zürich, Switzerland [9]Pediatric Nephrology Unit, Alexandria Faculty of Medicine, University of Alexandria, Alexandria, Egypt [10]Department of General Pediatrics, Adolescent Medicine and Neonatology, Medical Center - University Freiburg, Faculty of Medicine, University of Freiburg, Freiburg, Germany [11]Department of Pediatrics, University Children's Hospital Berlin, University Hospital Berlin Charité, Berlin, Germany [12]University of Zagreb School of Medicine, University Hospital Center Zagreb, Zagreb, Croatia [13]Department of Genetics, Yale University School of Medicine, New Haven, Connecticut, USA [14]Yale Center for Mendelian Genomics, Yale University School of Medicine, New Haven, Connecticut, USA

Correspondence should be addressed to: Friedhelm Hildebrandt, M.D., Division of Nephrology, Boston Children's Hospital, 300 Longwood Avenue, Boston, Massachusetts 02115, Phone: +1 617-355-6129, Fax: +1 617-730-0365, friedhelm.hildebrandt@childrens.harvard.edu.

[¶]These authors contributed equally to this work.

AUTHOR CONTRIBUTIONS

T.J.S. and F.Hildebrandt designed the study; T.J.S., V.K., A.M., S.S., F.B., I.O. performed WES analysis. T.J.S., V.K., M.T., B.S., J.F. performed experiments. T.J.S., V.K., M.T., J.F.H., P.M.K., S.A. and F.Hildebrandt analyzed the data. R.T., S.H., F.Hafeez, F.E., M.G., G.F.L., H.F. M.P., J.G., D.M. and M.A.B. recruited patients and obtained clinical data. S.M. and R.P.L. designed WES experiments. T.J.S., V.K., P.M.K. and S.A. made the figures. T.J.S., V.K. and F.Hildebrandt drafted and revised the paper; all authors approved the final version of the manuscript.

STATEMENT OF DISCLOSURE

None of other authors have competing financial interests to disclose.

Supplemental Material

Supplementary information is available at *Kidney International's* website

Abstract

Distal renal tubular acidosis is a rare renal tubular disorder characterized by hyperchloremic metabolic acidosis and impaired urinary acidification. Mutations in three genes (*ATP6V0A4, ATP6V1B1* and *SLC4A1)* constitute a monogenic causation in 58–70% of familial cases of distal renal tubular acidosis. Recently, mutations in *FOXI1* have been identified as an additional cause. Therefore, we hypothesized that further monogenic causes of distal renal tubular acidosis remain to be discovered. Panel sequencing and/or whole exome sequencing was performed in a cohort of 17 families with 19 affected individuals with pediatric onset distal renal tubular acidosis. A causative mutation was detected in one of the three "classical" known distal renal tubular acidosis genes in 10 of 17 families. The seven unsolved families were then subjected to candidate whole exome sequencing analysis. Potential disease causing mutations in three genes were detected: *ATP6V1C2*, which encodes another kidney specific subunit of the V-type proton ATPase (1 family); *WDR72* (2 families), previously implicated in V-ATPase trafficking in cells; and *SLC4A2* (1 family), a paralog of the known distal renal tubular acidosis gene *SLC4A1.* Two of these mutations were assessed for deleteriousness through functional studies. Yeast growth assays for *ATP6V1C2* revealed loss-of-function for the patient mutation, strongly supporting *ATP6V1C2* as a novel distal renal tubular acidosis gene. Thus, we provided a molecular diagnosis in a known distal renal tubular acidosis gene in 10 of 17 families (59%) with this disease, identified mutations in *ATP6V1C2* as a novel human candidate gene, and provided further evidence for phenotypic expansion in *WDR72* mutations from amelogenesis imperfecta to distal renal tubular acidosis.

Graphical Abstract

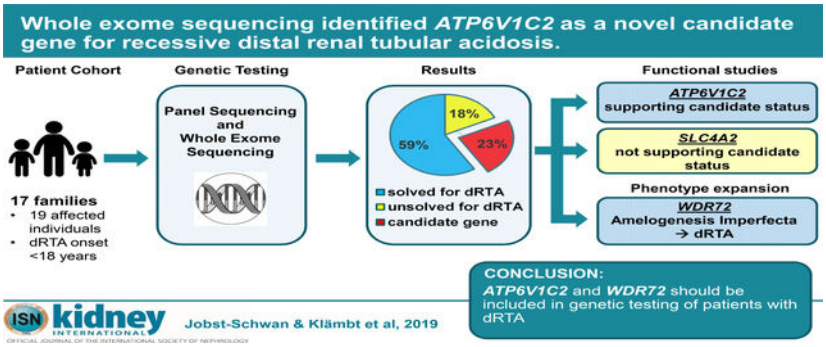

Keywords

distal tubule; renal acidification; renal tubular acidosis; pediatric nephrology

INTRODUCTION

Distal renal tubular acidosis (dRTA) is a rare renal tubular disorder characterized by hyperchloremic, hypokalemic metabolic acidosis accompanied by impaired urinary acidification. In many cases, this metabolic condition leads to growth retardation, osteomalacia, severe muscle weakness, nephrolithiasis, nephrocalcinosis (NC), and, if untreated, progression to renal failure.[1, 2] While the major causes of dRTA in adults are autoimmune diseases, childhood onset dRTA is mainly due to monogenic mutations.

Mutations in the genes *ATP6V0A4* and *ATP6V1B1,* both encoding subunits of the V-type proton ATPase, are causative in the majority of recessive cases of dRTA and are often accompanied by sensorineural deafness (SD) due to gene co-expression in the inner ear.[1, 3, 4] Mutations in *SLC4A1* have been identified as causative for autosomal recessive as well as dominant cases of dRTA without SD.[5] These 3 "classical genes" account for 58–70% of familial dRTA cases,[1, 6] suggesting the existence of yet undefined monogenic causes of dRTA. Accordingly, mutations in the gene *FOXI1* have been identified in 2 families with dRTA and functional studies of the mutation show loss-of-function of the variant.[7] Furthermore, very recently *WDR72* mutations have been proposed to expand the human phenotype of amelogenesis imperfecta (AI) by dRTA,[8, 9] underlining the potential for further identification of novel dRTA disease genes.

In order to identify novel monogenic causes for dRTA, we performed panel sequencing and/or whole exome sequencing (WES) in a cohort of 19 affected individuals from 17 families diagnosed with pediatric onset dRTA of unassigned molecular diagnosis. 10 of the 17 families had been prescreened for the 3 classical dRTA genes by gene panel sequencing. The unsolved cases, and all patients recruited subsequently, were subject to WES. This sequential procedure allowed diagnosis of mutations in 1 of the 3 classical dRTA genes in 10/17 families (59%). Furthermore, we identified novel mutations in *WDR72* in 2 families with dRTA and AI, and in 2 potential novel dRTA genes in 2 families: *ATP6V1C2*, and *SLC4A2*. Functional studies for *ATP6V1C2* and *SLC4A2* were performed, and were conclusive for loss-of-function for the *ATP6V1C2* mutation.

RESULTS

We evaluated 19 affected individuals from 17 families with clinically diagnosed dRTA that presented before the age of 25 years (Fig. 1). Among these 19 individuals, 17 had NC or renal stones and 8 presented with SD (Table 1). 10 families were reported to be consanguineous. Initial panel screening was performed by multiplex PCR in 11 individuals from 10 families for the 3 classical dRTA genes (*ATP6V0A4, ATPV1B1, SLC4A1*). Genomic DNAs of the 3 families not solved by panel sequencing and 7 additional families subsequently recruited were then subjected to WES (Fig. 1).

Known genes

Using our established evaluation based on ACMG criteria for deleteriousness for alleles of monogenic disease genes[10] we identified likely causative mutations in 10/17 families (59%) in 1 of the 3 classical dRTA genes (Figure 1, Table 1). Specifically, we identified recessive mutations in *ATP6V0A4* (NM_020632.2) in 3 families (4 individuals) and in *ATP6V1B1* (NM_001692.3) in 4 families (4 individuals), and *SLC4A1* (NM_000342.2) mutations in 3 families (3 individuals, 1 recessive homozygous, 1 recessive compound heterozygous, 1 dominant heterozygous mutation) (Table 1). 9 of the 10 identified mutations had been previously reported. The homozygous mutation in *ATP6V0A4* in family F589 (*c.2446A>G*, p.Lys816Glu) is a novel mutation affecting a lysine that has been conserved throughout evolution starting from yeast. The mutation has strong prediction scores and is unreported in

either homozygous or heterozygous state in the healthy exome and genome database gnomAD (Table 1).

ATP6V1C2

In the 7 dRTA cases in whom no causative mutation was found, we performed WES analysis and utilized the WES datasets for homozygosity mapping to evaluate consanguineous cases for homozygous recessive mutations within homozygous haplotypes.[11] We identified a very likely deleterious recessive mutation in the gene *ATP6V1C2* (NM_001039362.1) in family F588 (Fig. 2A, Table 2, Suppl. Fig. S1A). Like *ATP6V0A4* and *ATP6V1B1, ATP6V1C2* encodes a subunit (subunit C) of the V-type proton ATPase (Fig. 3A).[12] In contrast to its paralog *ATP6V1C1, ATP6V1C2* is predominantly expressed in the kidney with high expression in renal intercalated cells (IC) (Fig. 2D).[13, 14] The gene has been implicated as a human candidate disease gene for dRTA but no mutations have been identified so far.[14] The mutation *c.503T>C*, p.Ile168Thr changes the nonpolar aa residue Ile to the polar Thr. Alignment of the orthologs protein sequences reveals evolutionary conservation of Ile or the biochemically similar Leu from yeast to humans (Fig. 2A). Ile168 is located in a hydrophobic knuckle (Suppl. Fig. S2) that slides against another hydrophobic surface of the C-subunit during the ATPase catalytic cycle.[15] We modeled this human mutation in the yeast ortholog *VMA5* (YKL080W) that encodes the yeast V-ATPase C subunit and introduced the corresponding mutation (p.Ile178Thr) into the genomic copy of *VMA5* to obtain *vma5* p.Ile178Thr mutant strains. Thermal protein stability was predicted for the 3 states of Vma5 reported by Zhao *et al.*[15] Protein stability prediction (CUPSAT) suggests stabilization of state 1 (Suppl. Fig. S3A) but destabilization of state 2 (Suppl. Fig. S3B) and state 3 (Suppl. Fig. S3C).[16] These results predict stabilization of the protein in state 1, possibly preventing the dynamic conformational changes likely required for stable function of the active ATPase.

To further assess loss-of-function of the p.Ile168Thr mutation in *ATP6V1C2* (p.Ile178Thr in yeast *vma5*), we tested the growth of 3 independent mutant isolates compared to wild-type (WT) cells grown on YEPD medium buffered to pH 5 and on YEPD medium buffered to pH 7.5 containing 60 mM $CaCl_2$ (Fig. 3B). Vma mutants with no V-ATPase activity are able to grow at pH 5, while an elevated pH or Ca^{2+} concentration is lethal to yeast mutants lacking the V-ATPase activity.[17, 18] Here, we showed that *vma5* (Ile178Thr) mutant indeed failed to grow on YEPD, pH 7.5 +$CaCl_2$ plates, suggesting a significant loss of V-ATPase function (Fig. 3B).

To further explore the source of the growth defect, we isolated vacuolar vesicles from WT and mutant yeast strains. Vacuolar vesicles isolated from 3 independent mutant strains had concanamycin A-sensitive V-ATPase activity, but this activity was much lower than V-ATPase activity in WT vacuoles (Figure 3C), We visualized the levels of both membrane-bound (vacuolar V_0 subunit a, Vph1) and peripheral V_1 subunits (A, B, and C) by immunoblot. Importantly, the V_0 and V_1 subcomplexes can assemble independently and the V_0 subcomplex reaches the vacuole even in the complete absence of V_1 subunits. Consistent with this, the levels of V_0 subunit Vph1, ortholog of human subunit a (Fig. 3A) were comparable between the WT and mutant strains (Fig. 3D), indicating that the V_0 complex is correctly assembled and transported to the vacuole. In contrast, the level of the Vma5

protein in the mutant vacuolar vesicles was reduced, as were the levels of V_1 subunits A and B (Fig. 3D). By immunoblot of whole cell lysates, we investigated whether the reduced Vma5 levels reflected impaired V-ATPase assembly or poor stability of the mutant Vma5 polypeptide (Fig. 3E). Vma5 protein was barely detectable in whole cell lysates from mutant *vma5* Ile178Thr, suggesting protein instability. However, the low detectable levels of vma5 Ile178Thr in vacuolar vesicles indicate that mutant Vma5 can assemble into V-ATPase at the vacuole (Fig. 3D).

WDR72

In 2 additional dRTA families (F382 and B2673; 3 individuals), we identified homozygous mutations in the gene *WDR72* (NM_182758.3), located in a segment of homozygosity by descent (Fig. 2B, Fig. 4, Suppl. Fig. S1B–D, Table 2). WDR72 is a paralog of WDR7 which interacts with human dRTA protein ATP6V1B1 and co-localizes with V-ATPases in IC. WDR7 was shown to promote V-ATPase activity and to mediate intracellular vesicle acidification.[19] WDR72 may function similarly. The mutation c.477_485dup, p.Ile159_Cys161dup showed recessive segregation within family F382 and is predicted to cause an in-frame insertion of 3 aa in the third WD40 domain of WDR72 (Fig. 2B, Fig. 4A). In family B2673 with 2 affected siblings with dRTA (Fig. 4C), the homozygous mutation c.764_768delGGCAG, p.Gly255Valfs*40 results in a premature stop codon and is a presumptive loss-of-function variant. Neither mutation was reported in the gnomAD database in a homozygous state. Single cell RNA sequencing databases indicate that *WDR72* is highly expressed in IC (Fig. 2D). *WDR72* mutations can cause autosomal recessive amelogenesis imperfecta (AI) in humans[20] and mice.[21] Very recently, 4 families with association of dRTA and AI and a *WDR72* mutation have been described.[8, 9] Interestingly, upon “reverse phenotyping” by contacting our clinical collaborators, we learned that all of our here described *WDR72* mutant subjects have distinct features of AI as well (Fig. 4, Table 2). We thereby confirmed that *WDR72* mutations can be associated with a syndromic disease of AI and dRTA.[8,9]

SLC4A2

In family F588 we identified a homozygous missense mutation in the gene *SLC4A2* (NM_01199692.2), located within a segment of homozygosity by descent (Table 2, Fig. 2C, Suppl. Fig. S1E). *SLC4A2* encodes the Anion Cl^-/HCO_3^- exchanger 2 (AE2) and is a paralog of the known dRTA gene *SLC4A1* encoding a basolateral Cl^-/HCO_3^- exchanger of the collecting duct Type A IC. The *SLC4A2* locus was previously proposed as a recessive dRTA candidate gene on the basis of genetic linkage to a 14 Mb region of chromosome 7q, but no disease causing mutation could be confirmed at that time.[22] The *SLC4A2* mutation c.2107G>A, p.Ala703Thr in family F588 replaces the short hydrophobic side chain of Ala703 with a longer, more hydrophilic side chain which may alter its predicted interaction with hydrophobic residue Ile761 (Suppl. Fig. S4). Indeed, CUPSAT[17] predicts a destabilizing effect of the Ala703Thr substitution as modeled on the crystal structure of the human *SLC4A1* paralog transmembrane domain (Suppl. Fig. S5).[16, 23]

To test the deleteriousness of the Ala703Thr missense mutation, we generated the corresponding human (hAE2) and mouse (mAE2) cDNA constructs. Transient expression of

WT hAE2 in MDCKII cells showed the expected predominant peripheral membrane localization (Fig. 5A, C) which was unaltered in cells expressing hAE2 Ala703Thr (Fig. 5B, D), suggesting unimpaired biosynthetic trafficking in this context. The trafficking similarities of HA-tagged and untagged hAE2 polypeptides was reflected in comparable $^{36}Cl^-$ uptake activities of cRNA-injected *Xenopus laevis* oocytes (Suppl. Fig. S6A). Additional assays of functional expression in *Xenopus* oocytes revealed hAE2 Ala703Thr-mediated Cl^-/HCO_3^- and Cl^-/Cl^- exchange activities sensitive to the stilbene disulfonate inhibitor, DIDS, that were indistinguishable from those of WT hAE2 (Fig. 5E, F). The extracellular pH-dependence of hAE2-mediated Cl^-/Cl^- exchange was similar to that of WT hAE2 (Fig. 5G, H). Moreover, WT hAE2 activations by acidic intracellular pH (Suppl. Fig. S7) and by hypertonicity (Suppl. Fig. S8) were indistinguishable in oocytes expressing hAE2 Ala703Thr. The 2.4 mM $K_{1/2}$ for extracellular Cl^- exhibited by WT hAE2 was identical to that of the mutant (Suppl. Fig. S9). NH_4^+-stimulated hAE2-mediated, DIDS-sensitive Cl^-/Cl^- exchange was slightly reduced compared to WT hAE2 (Suppl. Fig. S10), but not to a degree that would imply pathological significance.

In summary, as variant A703T did not relevantly alter AE2 function in the multiple experimental conditions tested, our data failed to support *SLC4A2* as a viable dRTA candidate gene.

DISCUSSION

To identify potential additional monogenic causes of dRTA, we performed panel sequencing and/or WES combined with homozygosity mapping in 17 families with clinically diagnosed childhood onset dRTA. In 10/17 families (59%), we identified causative mutations in 1 of the 3 known, classical dRTA genes. In addition, we discovered potentially disease-causing mutations the 3 genes *ATP6V1C2, WDR72* and *SLC4A2,* and functionally evaluated the mutations in *ATP6V1C2* and *SLC4A2*. These studies confirmed *ATP6V1C2* as a novel recessive dRTA candidate gene, confirmed expansion of the phenotypic spectrum of AI due to *WDR72* mutations, but failed to detect functional evidence supporting the genetic data that suggested *SLC4A2* as a candidate dRTA gene.

Genetic testing of our cohort provided a molecular diagnosis for 59% of all cases with a clinical dRTA phenotype, a percentage comparable to that of Ashton *et al* (57%)[6] among European children, but lower than that of Palazzo *et al* (70%)[1] among Italian children.

WES and homozygosity mapping initially identified *ATP6V1C2, WDR72*, and *SLC4A2* as potential novel dRTA genes. Candidate status of all 3 genes was supported by high expression levels of each in the renal IC cluster in single cell mRNA sequencing data (Fig. 2D).[24]

As for known dRTA disease genes *ATP6V0A4* and *ATP6V1B1,* the novel candidate gene *ATP6V1C2* is a subunit of the V-type H^+- ATPase. We showed the yeast *Vma5* V-ATPase C subunit mutation p.Ile178Thr corresponding to human *ATP6V1C2* mutation Ile168Thr had properties of a loss-of-function mutation (Fig. 3). Yeast strains expressing the mutant C subunit showed reduced V-ATPase activity and exhibited a Vma5 growth phenotype.

Although the mutant C subunit was slightly detectable in isolated vacuolar vesicles, it was not detectable in whole cell lysates and V-ATPase complexes were insufficient to support full V-ATPase function (Fig. 3). Therefore, these findings suggest loss-of-function for the corresponding human mutation *c.503T>C*, p.Ile168Thr, and confirm *ATP6V1C2* as a novel dRTA candidate gene.

We also identified 2 novel homozygous *WDR72* mutations in 2 families with dRTA and AI (Fig. 2B, Fig. 4). Mutation c.764_768delGGCAG encodes a frameshift leading to an early stop codon, and therefore can be considered a loss-of-function variant. The second mutation encodes a 3 aa insertion within the third WD40 domain of WDR72 (Fig. 2B). In genome-wide association studies, *WDR72* has been associated with loss-of kidney function and chronic kidney disease.[25, 26] Recessive mutations in *WDR72* are a known cause for AI (OMIM 613211), causing vesicle trafficking defects in ameloblasts and thereby impairing enamel formation.[20, 27] The association of AI and dRTA has been described very recently in 4 families with *WDR72* mutations.[8, 9] *WDR72* mutations may thus underlie several dRTA cases with accompanying dental abnormalities reported without molecular diagnosis.[28–30]

The biological function of WDR72 is still largely unknown. *Wdr72*$^{-/-}$ mice mimic the human enamel defect[31] but the renal phenotype has not been investigated to date. WDR72 is an intracellular protein, with a predicted structure including N-terminal WD40 repeats forming 2 β-propellers and a C-terminal α-solenoid tail. WDR7, a human paralog of WDR72, regulates Ca^{2+}-dependent exocytosis of neurotransmitter release at synapsis.[32] Furthermore, WDR7 interacts with human dRTA protein ATP6V1B1 and co-localizes with V-ATPases in IC. WDR7 was shown to promote V-ATPase activity and to mediate intracellular vesicle acidification.[19] WDR72 may have similar functions in IC with involvement in vesicle trafficking. However, further investigations into the pathogenesis of *WDR72* mutations in dRTA are warranted. Our findings have thus confirmed the phenotypic expansion of *WDR72* mutations from isolated AI to a syndromic disease that features both AI and dRTA.[8]

SLC4A2 encodes the AE2 Cl^-/HCO_3^- exchanger and is a paralog of the known dRTA gene *SLC4A1* encoding a basolateral Cl^-/HCO_3^- exchanger of the collecting duct Type A IC. Moreover, *Slc4a2* was cloned from and immunolocalized in guinea pig cochlea,[33] and *SLC4A2* mRNA was detected in cochlear epithelial cells differentiated from human iPSC.[34] A dRTA disease gene region was mapped by linkage analysis in 9 dRTA families to a 14 cM region of human chromosome 7q33–34 encompassing the *SLC4A2* gene.[22] We identified a missense mutation in *SLC4A2* in an unbiased candidate approach by WES in a patient with dRTA and hearing loss. However, functional expression of human or mouse AE2 protein in *Xenopus* oocytes revealed no significant functional differences between WT and mutant proteins in baseline Cl^-/HCO_3^- or Cl^-/Cl^- exchange activities or in Cl^-/Cl^- exchange regulation by intracellular or extracellular pH, by hypertonicity, or by ammonium (Fig. 5, Suppl. Fig. S6–S10). These experiments did not exclude the possibility that the mutation impairs activity or regulated expression of AE2 in IC *in situ* or in another model epithelial cell type grown in different conditions.[35]

Slc4a2 knock-out (KO) mice are toothless, are severely growth-retarded, develop achlorhydria and abnormal gastric epithelium, and die within the first 40 days of life.[36] Although the patient lacks these features of the mouse KO phenotype, a hypomorphic missense mutation might not resemble a KO.

SLC4A2 residue 703 corresponds to SLC4A1 residue 400. Heterozygous deletion of residues 400–408 causes the benign hematological condition, Southeast Asian Ovalocytosis (SAO), without renal phenotype. However, the rare homozygous SAO deletion is associated with severe dyserythropoietic hemolytic anemia and dRTA,[37] and causes anemia and dRTA in compound heterozygous states as well. SLC4A2 Ala703 is located at the C-terminal end of AE2's N-terminal cytoplasmic domain, near the start of the first of AE2's 14 transmembrane helices. The missense mutation p.Ala703Thr is predicted to possibly interfere with protein stability (Suppl. Fig. S4),[16] through a conformational change in the flexible linker region connecting cytoplasmic and transmembrane domains, as in AE1,[38] or through potentially altered modulation by proteinase CK2 or other regulators.[39] In summary, no significant hAE2 loss-of-function resulted from the c.2107G>A substitution allele, as detected by our assays. Identification of additional dRTA patients with *SLC4A2* mutations and further experimental studies will be necessary to maintain *SLC4A2* as a candidate disease gene for dRTA and hearing loss.

We have presented combined panel sequencing and WES for the rapid and reliable molecular diagnosis of patients with a clinical diagnosis of dRTA. However, panel sequencing had been performed before the publication of both papers that associated *WDR72* mutations with dRTA. Thus, this temporal connection underlines the advantages of WES over panel sequencing as unsolved WES datasets may be reevaluated after discovery of novel genetic causes of the disease. As costs for WES are declining rapidly, WES should be considered as a first choice for genetic testing. Furthermore, we have established *ATP6V1C2* as a novel recessive dRTA gene in humans, and confirmed the phenotype expansion of recessive *WDR72* mutations from isolated AI to syndromic AI with dRTA. However, our functional data failed to reinforce the genetic evidence supporting *SLC4A2* as a candidate dRTA gene. Thus, WES provides a powerful tool to identify novel dRTA genes and, by directing functional validation studies, helps elucidate pathogenic mechanisms of dRTA.

METHODS

Study participants and genetic testing

This study was approved by the institutional review board (IRB) of Boston Children's Hospital (BCH). We obtained informed consent, clinical data, pedigree information, and DNA samples from subjects clinically diagnosed with dRTA manifesting before the age of 25 years.

Panel screening was performed by multiplex PCR for the genes *ATP6V1B1*, *ATP6V0A4* and *SLC4A1* in 11 individuals from 10 families as previously described.[40, 41] WES was performed as previously described[42] in 11 individuals from 10 families including 3

individuals from 3 families unsolved by panel sequencing. A mean depth of coverage of the known dRTA and candidate genes of 79.9X was achieved (Suppl. Table 1).

Homozygosity mapping was calculated based on whole exome sequencing data. In brief, aligned BAM files were processed using Picard and SAMtools as described by other groups.[43] Single nucleotide variant calling was performed using Genome Analysis Tool Kit (GATK).[44] The resulting VCF files were used to generate homozygosity mapping data and visual outputs using the program Homozygosity Mapper.[45]

Variants were evaluated for mutations in known dRTA genes. Remaining variants were ranked based on their predicted impact on protein sequence and function considering evolutionary conservation among orthologs across phylogeny, and web-based pathogenicity prediction programs (PolyPhen-2[46], SIFT[47] and MutationTaster[48]). Remaining variants were evaluated by literature review and by phenotype correlation. Deleteriousness was assessed using on our established criteria based on ACMG.[10] Unsolved WES datasets were subjected to candidate gene analysis. Remaining variants were confirmed in original patient DNA by Sanger sequencing as previously described (Suppl. Fig. S11).[49] Whenever parental DNA was available, segregation analysis was performed.

Yeast growth assay

The *ATP6V1C2* mutation isoleucine 178 to threonine (vma5I178T) that reflects the human mutation Ile168Thr was introduced into the genomic copy of *VMA5* in WT yeast strain SF838–5Aα by a variation of the delitto perfetto method.[50] AA 150–214 of *VMA5* were replaced with *URA3*, and transformants were selected on fully supplemented minimal medium lacking uracil.[51] The I178T mutation was first introduced into a plasmid borne copy of WT VMA5 by Quikchange mutagenesis (Agilent) using oligonucleotides VMA5 I178T forward 5'CTGTCAGATCCTTGCATGATACTGTCAAGCCCGAAGACTTCGTTC-3' and VMA5 I178T reverse 5'GAACGAAGTCTTCGGGCTTGACAgTATCATGCAAGGATCTGACAGAAAG-3', introduction of the mutation was confirmed by sequencing. A *VMA5* fragment containing the I178T mutation was then PCR-amplified and used to transform the *vma5Δ*150–214::*URA3* strain. Transformants that had replaced *URA3* with the mutated fragment were selected on medium containing 5-fluoro-orotic acid (5-FOA), which selects against the *URA3* marker. 3 separate transformants that grew on 5-FOA but had lost growth on medium lacking uracil were analyzed further. Growth of WT and *vma5* (I175T) strains was compared by growing all strains to log-phase, diluting to 0.1 OD/ml and then doing sequential 10-fold serial dilutions of each strain before pinning onto YEPD plates buffered to pH 5 with 50 mM phosphate and 50 mM succinate or YEPD plates buffered to pH 7.5 containing 60 mM $CaCl_2$.

Isolation and characterization of vacuolar vesicles

Vacuolar vesicles were isolated as described previously.[52] ATPase activity was determined at 37°C through a coupled enzyme assay (V-ATPase activity was activity sensitive to 200 nM concanamycin A). Immunoblots were performed as described previously.[53] Vacuolar vesicles were solubilized in cracking buffer, and separated by SDS-PAGE, and transferred to

nitrocellulose. Mouse monoclonal antibodies 8B1, 13D11, and 10D7, were used to detect V_1 subunits A and B and Vph1, respectively. Vma5 (V_1 subunit C) was detected with rabbit polyclonal antiserum against Vma5 (a generous gift from Tom Stevens, University of Oregon). Whole cell lysates were obtained by several rounds glass bead lysis of cells in cracking buffer, followed by heating to 95°C. Lysates from 0.5 OD600 units of cells were probed for V_1 A and B as described above. Lysates probed for V_1C came from 2.5 oD600 units of cells.

Xenopus oocyte experiments

Construction and mutagenesis of cDNA expression plasmids—Mouse *Ae2a* (*Slc4a2*) was subcloned into the *Xenopus* oocyte expression vector pXT7 and used as previously described.[54] Human *AE2a* (*SLC4A2*) cDNA was purchased from OriGene and subcloned into pXT7. *SLC4A2* mutations mouse *Ae2* A699T and human *AE2* A703T were generated by four primer polymerase chain reaction (PCR) as described before.[55] All constructs were subcloned into pCDNA3 for transient transfection of MDCK cells.

Expression of cRNAs in *Xenopus* oocytes

Capped cRNA was transcribed from linearized cDNA templates with T7 polymerase (Ambion, Austin, TX). RNA integrity was confirmed by agarose gel electrophoresis in formaldehyde. Mature female *Xenopus* (Dept. of Systems Biology, Harvard Medical School; or NASCO, Madison, WI) were maintained and subjected to partial ovariectomy under hypothermic tricaine anesthesia following protocols approved by the Institutional Animal Care and Use Committee of Beth Israel Deaconess Medical Center. Stage V-VI oocytes were prepared by overnight incubation of ovarian fragments in MBS with 1.5 mg/ml collagenase B (Alfa Aesar), followed by a 20 min rinse in Ca^{2+}-free MBS with subsequent manual selection and defolliculation as needed. Oocytes were injected on the same day with cRNA (0.5–50 ng) or with water in a volume of 50 nl. Injected and uninjected oocytes were then maintained 2–6 days at 19°C in MBS [(in m M) 85 NaCl, 1 KCl, 2.4 $NaHCO_3$, 0.82 $Mg(SO_4)_2$, 0.33 $Ca(NO_3)_2$, 0.41 $CaCl_2$, and 10 HEPES (final pH 7.40)] containing gentamicin until used for experiments.

Isotopic influx experiments

$^{36}Cl^-$ influx studies were carried out in 96 well plates as previously described[56] for periods of 15, 20, or 30 min in ND-96 consisting of (in mM) 96 NaCl, 2 KCl, 1.8 $CaCl_2$, 1 $MgCl_2$, and 5 HEPES (pH 7.40). In Cl^--free ND-96 or in partial Cl^- substitution solutions, NaCl was replaced mole-for-mole with Na cyclamate or, as needed, the Cl^- salts of K^+, Ca^{2+}, and Mg^{2+} were substituted on an equimolar basis with the corresponding gluconate salts. Addition to flux media of the weak acid salt sodium butyrate (40 mM) was in equimolar substitution for Na cyclamate. Addition of NH_4Cl (20 mM) was in equimolar substitution for NaCl. In pH dependence experiments, 5 mM HEPES was replaced on an equimolar basis with a biological buffer of appropriate pKa: pH 5.0, MES; pH 6.0, MES; pH 7.0, HEPES; pH 8.0, HEPES; pH 9.0, CHES (pH adjusted with NaOH or HCl). Hypertonic solutions were formulated by addition of sodium chloride, sodium glutamate or mannitol as described,

and osmotic strength was measured by freezing point depression (Osmette A, Precision Systems Inc., Natick MA).

Bath volume was 150 μl and bath [Cl^-] was 103.6 mM, except as indicated in experiments conducted in hyperosmolar conditions. 0.25 μCi $^{36}Cl^-$ (ICN, Irvine, CA) was included in each well. Influx experiments were terminated with 3 washes in cold Cl^--free ND96, followed by oocyte lysis in 150 μl of 2% sodium dodecyl sulfate (SDS). 2 ml scintillation fluid (SX-18 ScintiVerse, Fisher) was added to each lysed oocyte, and radiation uptake was measured in a PerkinElmer Tri-Carb scintillation counter. Triplicate 10 μL aliquots of initial influx solution were used to calculate $^{36}Cl^-$ specific activity. Cl^- uptake by oocytes was calculated by comparing oocyte cpm to bath specific activity.

Isotopic efflux experiments

For unidirectional $^{36}Cl^-$ efflux studies, individual oocytes in Cl^--free ND-96 were injected with 50 nl of 260 mM Na36Cl (20,000–24,000 cpm). Following a 5 min recovery period in Cl^--free ND-96, the efflux assay was initiated by transfer of individual oocytes to 6 ml borosilicate glass tubes, each containing 1 ml efflux solution as specified. At intervals of 1 or 3 min, 0.95 ml of this efflux solution was removed for scintillation counting and replaced with an equal volume of fresh efflux solution. Following completion of the assay with a final efflux period either in Cl^--free cyclamate solution or in the presence of the inhibitor DIDS (200 μM), each oocyte was lysed in 150 μl of 2% SDS. Samples were counted for 3–5 min such that the magnitude of 2SD was <5% of the sample mean.

To vary pH_i, oocytes were pre-exposed to 40 mM Na butyrate (substituting for Na cyclamate) for 30 min prior to initiation of an efflux experiment, to acidify oocyte pH_i to pH ~6.7.[57] Upon removal of bath butyrate (with substitution by Na cyclamate) during the course of the efflux experiment, pH_i rapidly alkalinized back towards initial pH_i while pH_o remained constant. Variation of pH_o was achieved at near-constant pH_i. Some oocyte groups were exposed to 20 mM NH_4Cl during the course of efflux experiments, acidifying pH_i to pH_i 7.1–7.0.[58]

Efflux data were plotted as *ln* (% cpm remaining in the oocyte) vs. time. Efflux rate constants for $^{36}Cl^-$ were measured from linear fits to data from the last 3 time points sampled within each experimental period. For each experiment, water-injected or uninjected oocytes from the same frog were subjected to parallel measurements with cRNA-injected oocytes. Each experimental condition was tested in oocytes from at least 2 frogs. The following 2 exclusion criteria were defined for “non-specific” efflux or “leaky” oocytes in efflux experiments. One was <50% reduction in efflux rate constant in the presence of DIDS or in the absence of exchangeable bath anion. The second was loss of >85% of injected isotope prior to completion of the efflux assay.

Immunocytochemistry

MDCKII cells were plated on glass coverslips and transfected (Altogen Biosystems MDCK Transfection Reagent Kit) per manufacturer’s instructions. After 48 h cells on coverslip were fixed with 3% PFA in PBS for 30 min at room temperature (RT), then permeabilized with PBS + 0.1%(v/v) Triton X-100 for 15 min at RT, and blocked with PBS containing 2% BSA.

Primary antibodies used were rabbit polyclonal anti-mouse AE2 directed against C-terminal aa 1224–1237[59–61] and mouse monoclonal anti-HA tag (Cell Signaling), each overnight at 4°C at 1:2000 dilutions, then for 1 h at RT with secondary Cy3-conjugated goat anti-rabbit Ig or goat anti-mouse Ig (each at 1:1000 dilution).

Statistics

Data are reported as mean ± SE. Flux data were compared by Student's paired or unpaired 2-tailed T tests (Microsoft Excel), or by ANOVA with Tukey post-hoc analysis (SigmaPlot). pH dependence data were fit to a 4-parameter Hill equation in SigmaPlot 8.0.

Supplementary Material

Refer to Web version on PubMed Central for supplementary material.

ACKNOWLEDGEMENTS

We thank the physicians and the participating families for their contribution. We thank Leslie Speanas, Brittany Fisher, and Kassaundra Amann for recruitment of study participants. F.Hildebrandt is the William E. Harmon Professor of Pediatrics. This research was supported by grants from the National Institutes of Health DK1069274, DK1068306, and DK064614 to F.H. and 5U54HG006504 to R.P.L., and GM126020 to P.M.K.. T.J.S. (281319475), V.K. (403877094) and F.B. (404527522) are supported by the Deutsche Forschungsgemeinschaft. A.M. was supported by a NIH Training Grant in Pediatric Nephrology (T32DK007726), by the 2017 Post-doctoral Fellowship Grant from the Harvard Stem Cell Institute Kidney Group, and by the American Society of Nephrology Lipps Research Program 2018 Polycystic Kidney Disease Foundation Jared J. Grantham Research Fellowship. WES performed at Yale Center for Mendelian Genomics and Cologne Center for Genomics.

REFERENCES

1. Palazzo V, Provenzano A, Becherucci F, et al. The genetic and clinical spectrum of a large cohort of patients with distal renal tubular acidosis. Kidney Int 2017; 91: 1243–1255. [PubMed: 28233610]
2. Lopez-Garcia SC, Emma F, Walsh SB, et al. Treatment and long-term outcome in primary distal renal tubular acidosis. Nephrol Dial Transplant 2019.
3. Smith AN, Skaug J, Choate KA, et al. Mutations in ATP6N1B, encoding a new kidney vacuolar proton pump 116-kD subunit, cause recessive distal renal tubular acidosis with preserved hearing. Nature genetics 2000; 26: 71–75. [PubMed: 10973252]
4. Karet FE, Finberg KE, Nelson RD, et al. Mutations in the gene encoding B1 subunit of H+-ATPase cause renal tubular acidosis with sensorineural deafness. Nature genetics 1999; 21: 84–90. [PubMed: 9916796]
5. Bruce LJ, Cope DL, Jones GK, et al. Familial distal renal tubular acidosis is associated with mutations in the red cell anion exchanger (Band 3, AE1) gene. J Clin Invest 1997; 100: 1693–1707. [PubMed: 9312167]
6. Ashton EJ, Legrand A, Benoit V, et al. Simultaneous sequencing of 37 genes identified causative mutations in the majority of children with renal tubulopathies. Kidney Int 2018; 93: 961–967. [PubMed: 29398133]
7. Enerback S, Nilsson D, Edwards N, et al. Acidosis and Deafness in Patients with Recessive Mutations in FOXI1. J Am Soc Nephrol 2018; 29: 1041–1048. [PubMed: 29242249]
8. Rungroj N, Nettuwakul C, Sawasdee N, et al. Distal renal tubular acidosis caused by tryptophan-aspartate repeat domain 72 (WDR72) mutations. Clin Genet 2018; 94: 409–418. [PubMed: 30028003]
9. Zhang H, Koruyucu M, Seymen F, et al. WDR72 Mutations Associated with Amelogenesis Imperfecta and Acidosis. Journal of dental research 2019: 22034518824571.
10. Richards S, Aziz N, Bale S, et al. Standards and guidelines for the interpretation of sequence variants: a joint consensus recommendation of the American College of Medical Genetics and

Genomics and the Association for Molecular Pathology. Genet Med 2015; 17: 405–424. [PubMed: 25741868]

11. Hildebrandt F, Heeringa SF, Ruschendorf F, et al. A systematic approach to mapping recessive disease genes in individuals from outbred populations. PLoS Genet 2009; 5: e1000353. [PubMed: 19165332]
12. Sun-Wada GH, Wada Y. Role of vacuolar-type proton ATPase in signal transduction. Biochim Biophys Acta 2015; 1847: 1166–1172. [PubMed: 26072192]
13. Sun-Wada GH, Murata Y, Namba M, et al. Mouse proton pump ATPase C subunit isoforms (C2-a and C2-b) specifically expressed in kidney and lung. The Journal of biological chemistry 2003; 278: 44843–44851. [PubMed: 12947086]
14. Smith AN, Borthwick KJ, Karet FE. Molecular cloning and characterization of novel tissue-specific isoforms of the human vacuolar H(+)-ATPase C, G and d subunits, and their evaluation in autosomal recessive distal renal tubular acidosis. Gene 2002; 297: 169–177. [PubMed: 12384298]
15. Zhao J, Benlekbir S, Rubinstein JL. Electron cryomicroscopy observation of rotational states in a eukaryotic V-ATPase. Nature 2015; 521: 241–245. [PubMed: 25971514]
16. Parthiban V, Gromiha MM, Schomburg D. CUPSAT: prediction of protein stability upon point mutations. Nucleic acids research 2006; 34: W239–242. [PubMed: 16845001]
17. Forster C, Kane PM. Cytosolic Ca2+ homeostasis is a constitutive function of the V-ATPase in Saccharomyces cerevisiae. The Journal of biological chemistry 2000; 275: 38245–38253. [PubMed: 10991947]
18. Nelson H, Nelson N. Disruption of genes encoding subunits of yeast vacuolar H(+)ATPase causes conditional lethality. Proceedings of the National Academy of Sciences of the United States of America 1990; 87: 3503–3507. [PubMed: 2139726]
19. Merkulova M, Paunescu TG, Azroyan A, et al. Mapping the H(+) (V)-ATPase interactome: identification of proteins involved in trafficking, folding, assembly and phosphorylation. Scientific reports 2015; 5: 14827. [PubMed: 26442671]
20. El-Sayed W, Parry DA, Shore RC, et al. Mutations in the beta propeller WDR72 cause autosomal-recessive hypomaturation amelogenesis imperfecta. Am J Hum Genet 2009; 85: 699–705. [PubMed: 19853237]
21. Song W, Wang Y, Chu Q, et al. Loss of transforming growth factor-beta1 in epithelium cells affects enamel formation in mice. Archives of oral biology 2018; 96: 146–154. [PubMed: 30243146]
22. Karet FE, Finberg KE, Nayir A, et al. Localization of a Gene for Autosomal Recessive Distal Renal Tubular Acidosis with Normal Hearing (rdRTA2) to 7q33–34. The American Journal of Human Genetics 65: 1656–1665.
23. Arakawa T, Kobayashi-Yurugi T, Alguel Y, et al. Crystal structure of the anion exchanger domain of human erythrocyte band 3. Science 2015; 350: 680–684. [PubMed: 26542571]
24. Park J, Shrestha R, Qiu C, et al. Single-cell transcriptomics of the mouse kidney reveals potential cellular targets of kidney disease. Science 2018; 360: 758–763. [PubMed: 29622724]
25. Franceschini N, Haack K, Almasy L, et al. Generalization of associations of kidney-related genetic loci to American Indians. Clinical journal of the American Society of Nephrology : CJASN 2014; 9: 150–158. [PubMed: 24311711]
26. Kottgen A, Glazer NL, Dehghan A, et al. Multiple loci associated with indices of renal function and chronic kidney disease. Nature genetics 2009; 41: 712–717. [PubMed: 19430482]
27. Katsura KA, Horst JA, Chandra D, et al. WDR72 models of structure and function: a stage-specific regulator of enamel mineralization. Matrix Biol 2014; 38: 48–58. [PubMed: 25008349]
28. Misgar RA, Hassan Z, Wani AI, et al. Amelogenesis Imperfecta with Distal Renal Tubular Acidosis: A Novel Syndrome? Indian J Nephrol 2017; 27: 225–227. [PubMed: 28553046]
29. Ravi P, Ekambaranath TS, Arasi SE, et al. Distal renal tubular acidosis and amelogenesis imperfecta: A rare association. Indian J Nephrol 2013; 23: 452–455. [PubMed: 24339526]
30. Jain M, Agarwal MP, Wasir JS, et al. Amelogenesis imperfecta and distal renal tubular acidosis presenting as hypokalemic periodic paralysis. J Assoc Physicians India 1999; 47: 1205–1206. [PubMed: 11225229]

31. Wang SK, Hu Y, Yang J, et al. Critical roles for WDR72 in calcium transport and matrix protein removal during enamel maturation. Molecular genetics & genomic medicine 2015; 3: 302–319. [PubMed: 26247047]
32. Kawabe H, Sakisaka T, Yasumi M, et al. A novel rabconnectin-3-binding protein that directly binds a GDP/GTP exchange protein for Rab3A small G protein implicated in Ca(2+)-dependent exocytosis of neurotransmitter. Genes to cells : devoted to molecular & cellular mechanisms 2003; 8: 537–546. [PubMed: 12786944]
33. Stankovic KM, Brown D, Alper SL, et al. Localization of pH regulating proteins H+ATPase and Cl −/HCO3− exchanger in the guinea pig inner ear. Hear Res 1997; 114: 21–34. [PubMed: 9447915]
34. Hosoya M, Fujioka M, Sone T, et al. Cochlear Cell Modeling Using Disease-Specific iPSCs Unveils a Degenerative Phenotype and Suggests Treatments for Congenital Progressive Hearing Loss. Cell reports 2017; 18: 68–81. [PubMed: 28052261]
35. Mumtaz R, Trepiccione F, Hennings JC, et al. Intercalated Cell Depletion and Vacuolar H(+)-ATPase Mistargeting in an Ae1 R607H Knockin Model. Journal of the American Society of Nephrology : JASN 2017; 28: 1507–1520. [PubMed: 27932475]
36. Gawenis LR, Ledoussal C, Judd LM, et al. Mice with a targeted disruption of the AE2 Cl−/HCO3− exchanger are achlorhydric. The Journal of biological chemistry 2004; 279: 30531–30539. [PubMed: 15123620]
37. Picard V, Proust A, Eveillard M, et al. Homozygous Southeast Asian ovalocytosis is a severe dyserythropoietic anemia associated with distal renal tubular acidosis. Blood 2014; 123: 1963–1965. [PubMed: 24652967]
38. Jiang J, Magilnick N, Tsirulnikov K, et al. Single particle electron microscopy analysis of the bovine anion exchanger 1 reveals a flexible linker connecting the cytoplasmic and membrane domains. PloS one 2013; 8: e55408. [PubMed: 23393575]
39. Ibrahim SH, Turner MJ, Saint-Criq V, et al. CK2 is a key regulator of SLC4A2-mediated Cl(−)/HCO3(−) exchange in human airway epithelia. Pflugers Archiv : European journal of physiology 2017; 469: 1073–1091. [PubMed: 28455748]
40. Braun DA, Lawson JA, Gee HY, et al. Prevalence of Monogenic Causes in Pediatric Patients with Nephrolithiasis or Nephrocalcinosis. Clin J Am Soc Nephrol 2016; 11: 664–672. [PubMed: 26787776]
41. Halbritter J, Diaz K, Chaki M, et al. High-throughput mutation analysis in patients with a nephronophthisis-associated ciliopathy applying multiplexed barcoded array-based PCR amplification and next-generation sequencing. Journal of Medical Genetics 2012; 49: 756–767. [PubMed: 23188109]
42. Daga A, Majmundar AJ, Braun DA, et al. Whole exome sequencing frequently detects a monogenic cause in early onset nephrolithiasis and nephrocalcinosis. Kidney Int 2018; 93: 204–213. [PubMed: 28893421]
43. Li H, Handsaker B, Wysoker A, et al. The Sequence Alignment/Map format and SAMtools. Bioinformatics 2009; 25: 2078–2079. [PubMed: 19505943]
44. Van der Auwera GA, Carneiro MO, Hartl C, et al. From FastQ data to high confidence variant calls: the Genome Analysis Toolkit best practices pipeline. Current protocols in bioinformatics 2013; 43: 11 10 11–33. [PubMed: 25431634]
45. Seelow D, Schuelke M, Hildebrandt F, et al. HomozygosityMapper--an interactive approach to homozygosity mapping. Nucleic acids research 2009; 37: W593–599. [PubMed: 19465395]
46. Adzhubei IA, Schmidt S, Peshkin L, et al. A method and server for predicting damaging missense mutations. Nature methods 2010; 7: 248–249. [PubMed: 20354512]
47. Kumar P, Henikoff S, Ng PC. Predicting the effects of coding non-synonymous variants on protein function using the SIFT algorithm. Nature protocols 2009; 4: 1073–1081. [PubMed: 19561590]
48. Schwarz JM, Cooper DN, Schuelke M, et al. MutationTaster2: mutation prediction for the deep-sequencing age. Nature methods 2014; 11: 361–362. [PubMed: 24681721]
49. Otto EA, Ramaswami G, Janssen S, et al. Mutation analysis of 18 nephronophthisis associated ciliopathy disease genes using a DNA pooling and next generation sequencing strategy. J Med Genet 2011; 48: 105–116. [PubMed: 21068128]

50. Storici F, Resnick MA. The delitto perfetto approach to in vivo site-directed mutagenesis and chromosome rearrangements with synthetic oligonucleotides in yeast. Methods Enzymol 2006; 409: 329–345. [PubMed: 16793410]
51. Amberg DC, Botstein D, Beasley EM. Precise gene disruption in Saccharomyces cerevisiae by double fusion polymerase chain reaction. Yeast 1995; 11: 1275–1280. [PubMed: 8553698]
52. Roberts CJ, Raymond CK, Yamashiro CT, et al. Methods for studying the yeast vacuole. Methods Enzymol 1991; 194: 644–661. [PubMed: 1706462]
53. Kane PM, Kuehn MC, Howald-Stevenson I, et al. Assembly and targeting of peripheral and integral membrane subunits of the yeast vacuolar H(+)-ATPase. The Journal of biological chemistry 1992; 267: 447–454. [PubMed: 1530931]
54. Stewart AK, Kurschat CE, Burns D, et al. Transmembrane domain histidines contribute to regulation of AE2-mediated anion exchange by pH. American journal of physiology Cell physiology 2007; 292: C909–918. [PubMed: 17005605]
55. Clark JS, Vandorpe DH, Chernova MN, et al. Species differences in Cl− affinity and in electrogenicity of SLC26A6-mediated oxalate/Cl− exchange correlate with the distinct human and mouse susceptibilities to nephrolithiasis. The Journal of physiology 2008; 586: 1291–1306. [PubMed: 18174209]
56. Chernova MN, Jiang L, Shmukler BE, et al. Acute regulation of the SLC26A3 congenital chloride diarrhoea anion exchanger (DRA) expressed in Xenopus oocytes. The Journal of physiology 2003; 549: 3–19. [PubMed: 12651923]
57. Stewart AK, Chernova MN, Kunes YZ, et al. Regulation of AE2 anion exchanger by intracellular pH: critical regions of the NH(2)-terminal cytoplasmic domain. American journal of physiology Cell physiology 2001; 281: C1344–1354. [PubMed: 11546673]
58. Nakhoul NL, Hering-Smith KS, Abdulnour-Nakhoul SM, et al. Transport of NH(3)/NH in oocytes expressing aquaporin-1. American journal of physiology Renal physiology 2001; 281: F255–263. [PubMed: 11457716]
59. Gawenis LR, Bradford EM, Alper SL, et al. AE2 Cl−/HCO3− exchanger is required for normal cAMP-stimulated anion secretion in murine proximal colon. Am J Physiol Gastrointest Liver Physiol 2010; 298: G493–503. [PubMed: 20110461]
60. Stehberger PA, Shmukler BE, Stuart-Tilley AK, et al. Distal renal tubular acidosis in mice lacking the AE1 (band3) Cl−/HCO3− exchanger (slc4a1). J Am Soc Nephrol 2007; 18: 1408–1418. [PubMed: 17409310]
61. Alper SL, Stuart-Tilley AK, Biemesderfer D, et al. Immunolocalization of AE2 anion exchanger in rat kidney. Am J Physiol 1997; 273: F601–614. [PubMed: 9362338]
62. Stover EH, Borthwick KJ, Bavalia C, et al. Novel ATP6V1B1 and ATP6V0A4 mutations in autosomal recessive distal renal tubular acidosis with new evidence for hearing loss. J Med Genet 2002; 39: 796–803. [PubMed: 12414817]
63. Besouw MTP, Bienias M, Walsh P, et al. Clinical and molecular aspects of distal renal tubular acidosis in children. Pediatr Nephrol 2017; 32: 987–996. [PubMed: 28188436]
64. Bruce LJ, Wrong O, Toye AM, et al. Band 3 mutations, renal tubular acidosis and South-East Asian ovalocytosis in Malaysia and Papua New Guinea: loss of up to 95% band 3 transport in red cells. Biochem J 2000; 350 Pt 1: 41–51. [PubMed: 10926824]

Translational statement

Distal renal tubular acidosis (dRTA) causes metabolic acidosis, electrolyte imbalance and, if untreated, renal failure by mutations in 3 classical genes. We performed panel sequencing and/or whole exome sequencing in 17 dRTA families to identify novel genetic causes. In 10 families a molecular diagnosis in 1 of the 3 classical genes was established and in 4 families a dRTA candidate mutation (*ATP6V1C2, WDR72, SLC4A2*) was identified. Functional studies confirmed *ATP6V1C2* as a candidate gene, but excluded *SLC4A2*. Furthermore, we generated further evidence for a phenotypic expansion for *WDR72* mutations from amelogenesis imperfecta to dRTA. Thus, in future, *APT6V1C2* and *WDR72* mutations should be included in genetic testing for dRTA patients.

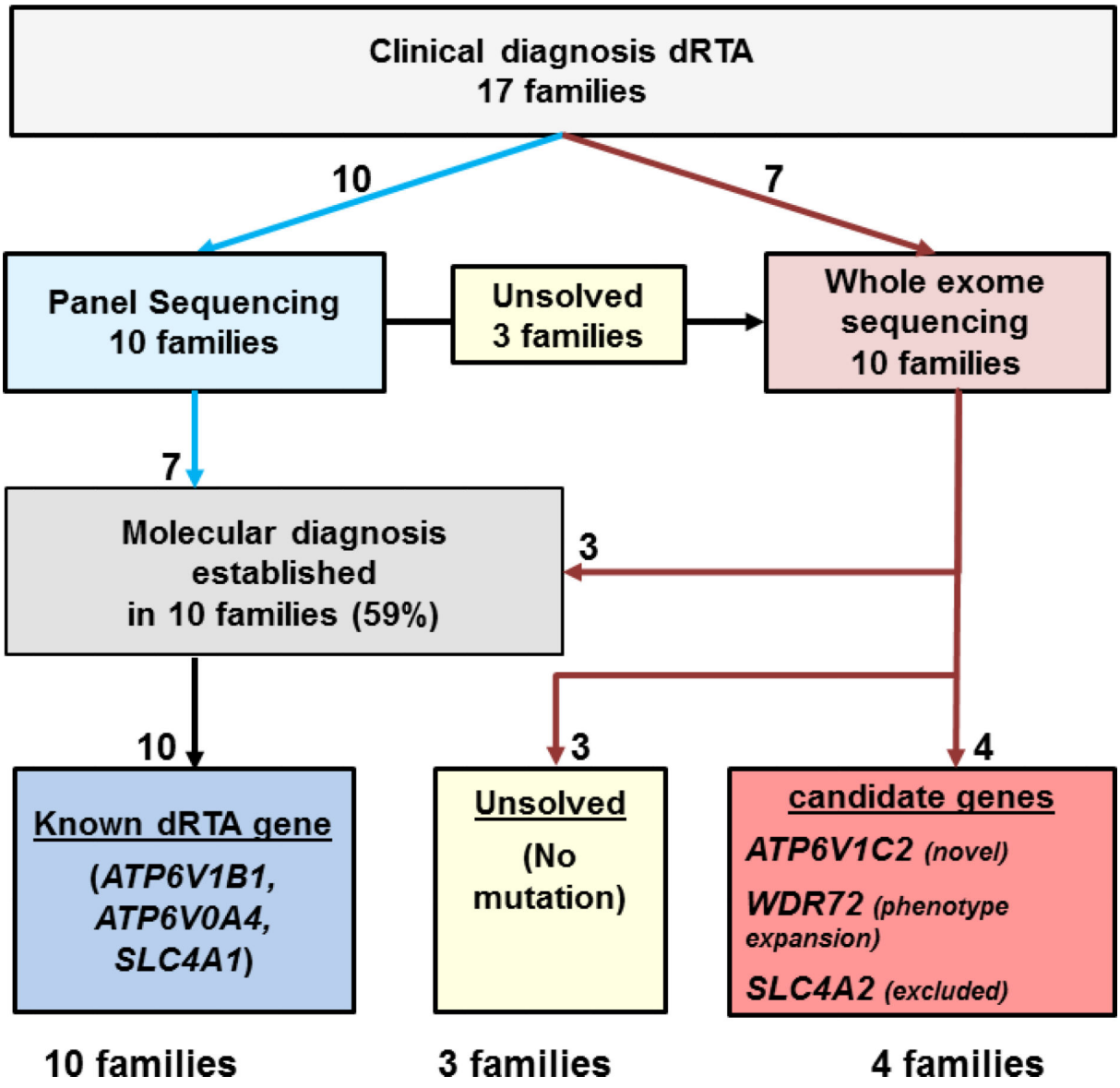

Figure 1: Flow Diagram for gene detection by panel sequencing and whole exome sequencing of likely causative monogenic mutations leading to distal renal tubular acidosis (dRTA), and candidate genes in 17 families.

By panel sequencing 10 families were tested for 3 known dRTA genes. Among those 10 families, 3 families were “unsolved” and assessed for whole exome sequencing, together with 7 additional families. A likely causative mutation in a known gene was detected in 10 families (59%) and in 4 families mutations indicating novel candidate dRTA genes were discovered.

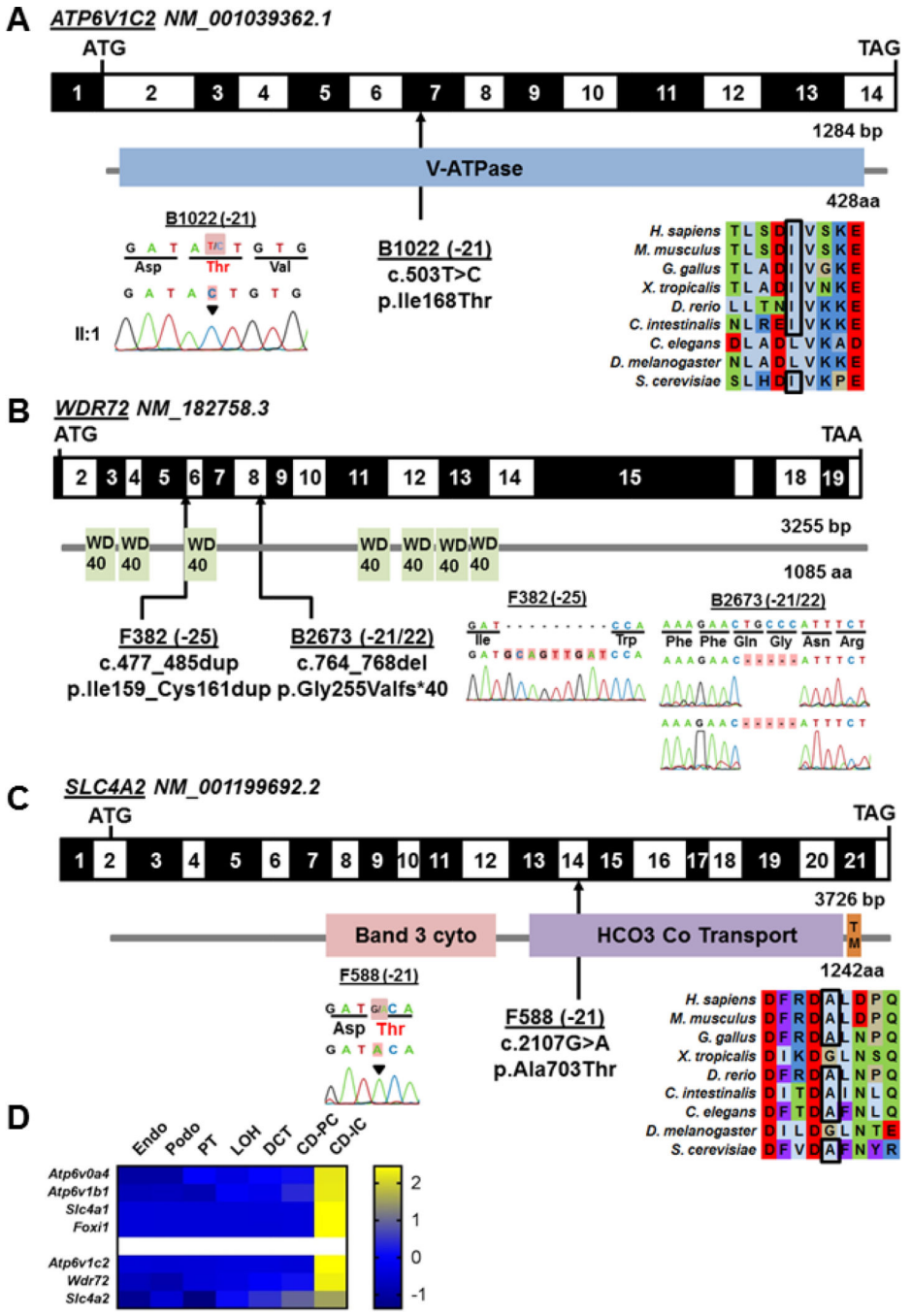

Figure 2: Whole exome sequencing in 4 families with dRTA identifies potentially disease-causing recessive mutations in 3 genes, *ATP6V1C2*, *WDR72*, and *SLC4A2*, that are expressed in intercalated cells.

Exon structure and protein domains of human *ATP6V1C2* (**A**), *WDR72* (**B**), and *SLC4A2* (**C**) cDNA. Positions of start codons (ATG) and stop codons (TAA, TGA) are indicated. Exon numbers are marked on a black or white background. Protein domain lengths are indicated by the colored boxes. Mutation positions are indicated by black arrows in relation to the exon and the protein domain (see also Table 1). Chromatograms of recessive mutations identified in dRTA patients are indicated under each protein domain diagram. **A-**

C. Black arrowheads or red highlights denote altered nucleotide. CLUSTAL-generated amino acid sequence alignments of *ATP6V1C2* and *SLC4A2* orthologs are shown for the regions surrounding sites of missense mutation (**A, C**). (**D**) Single cell type specific average expression of dRTA genes. Data was modified from Park *et al*.[24] The heat map is based on z-scores. Each column represents a cell type and each row represents one gene. aa: amino acid; bp: base pairs. Endo Endothelium, Podo Podocytes, PT proximal tubule, LOH loop of Henle, DCT distal convoluted tubule, CD-PC collecting duct - primary cells, CD-IC collecting duct - intercalated cells.

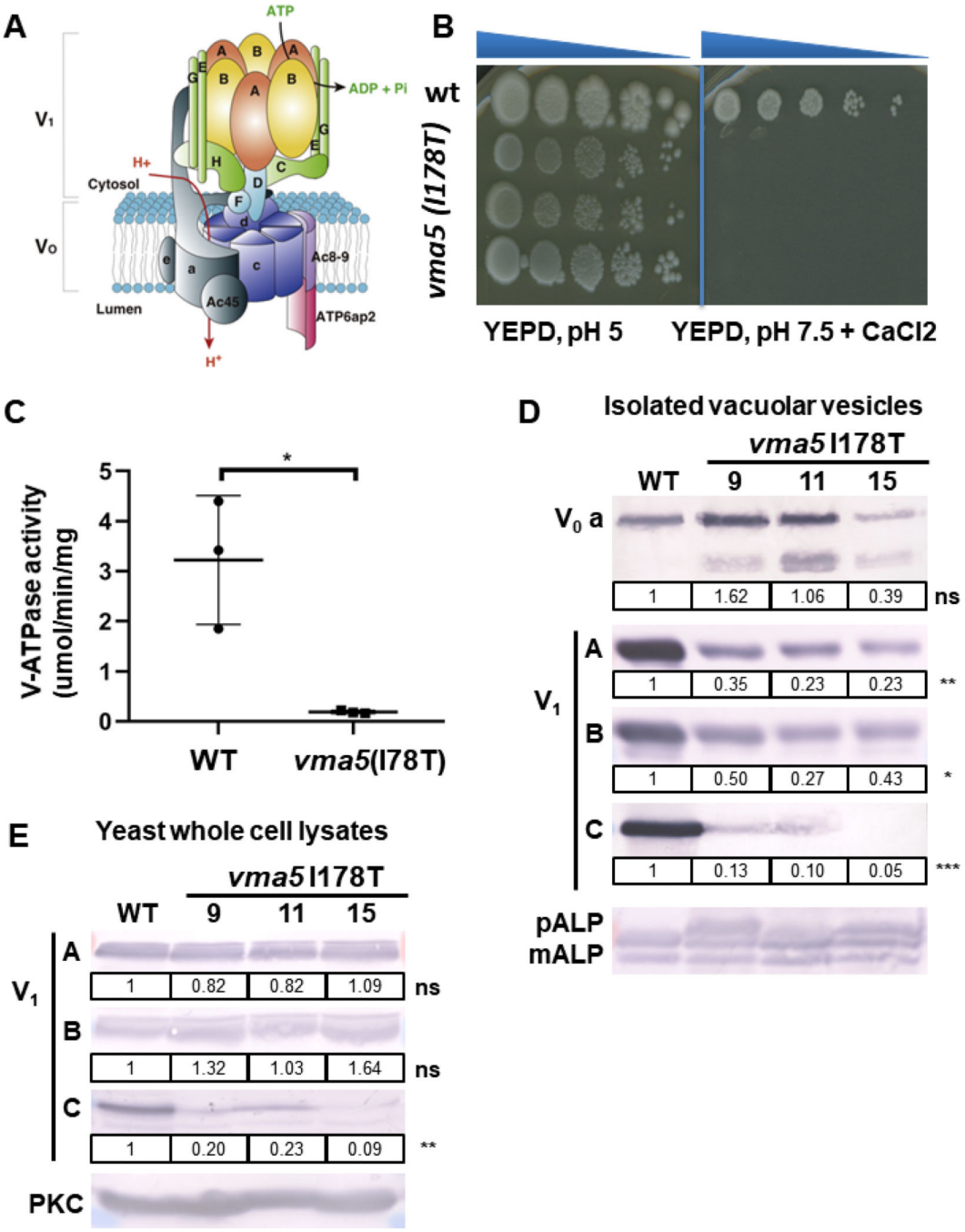

Figure 3: *vma5* (I178T) mutants display a growth defect and reduced V-ATPase activity.

(**A**) Structure of V-ATPase (modified from[12]) including a peripheral domain (V_1) important for ATP hydrolysis and an integral domain (V_0) responsible for proton translocation. The V_1 domain includes A and B subunits in a hexameric arrangement connected to the V_0 domain via peripheral stalks comprising subunits C, E, G, H and the N-terminal domain of subunit a. The V_0 domain includes a ring of proteolipids (c) adjacent to subunits a and e. (**B**) 3 independent isolates (9, 11, 15) containing the I178T *vma5* mutation fail to grow on YEPD, pH 7.5, $CaCl_2$ plates, whereas no growth loss was evident on YEPD, pH 5 plates. (**C**) Mean

concanamycin A-sensitive V-ATPase activity in vacuolar vesicles from WT and *vma5* I175T mutants (n=3 for each, error bars represent S.E.) (**D**) The levels of both membrane-bound (vacuolar V_0 subunit a, Vph1) and peripheral V_1 subunits (A, B, and C) were visualized by immunoblot and normalized to mature ALP (mALP), a vacuolar membrane protein. mALP runs as 2 bands as in the wild-type sample. If V-ATPase activity and therefore, vacuolar proteolytic activity, is reduced, a third higher molecular weigth pro-ALP band (pALP) appears, which is present in the mutants. The levels of Vph1 were similar in vacuolar vesicles prepared from 3 different mutant strains compared to WT (ns, P=0.94), but the level of the Vma5 protein was reduced (***, $P \leq 0.001$), as were the levels of the V_1 subunits, A (**, $P \leq 0.01$) and B (*, $P \leq 0.05$).

(**E**) V_1 subunits (A, B, and C) were measured via immunoblot in yeast whole cell lysates of WT and 3 different mutant strains and normalized to PKC as loading control. Levels of the C subunit are reduced in the mutant strains (**, $P \leq 0.01$).

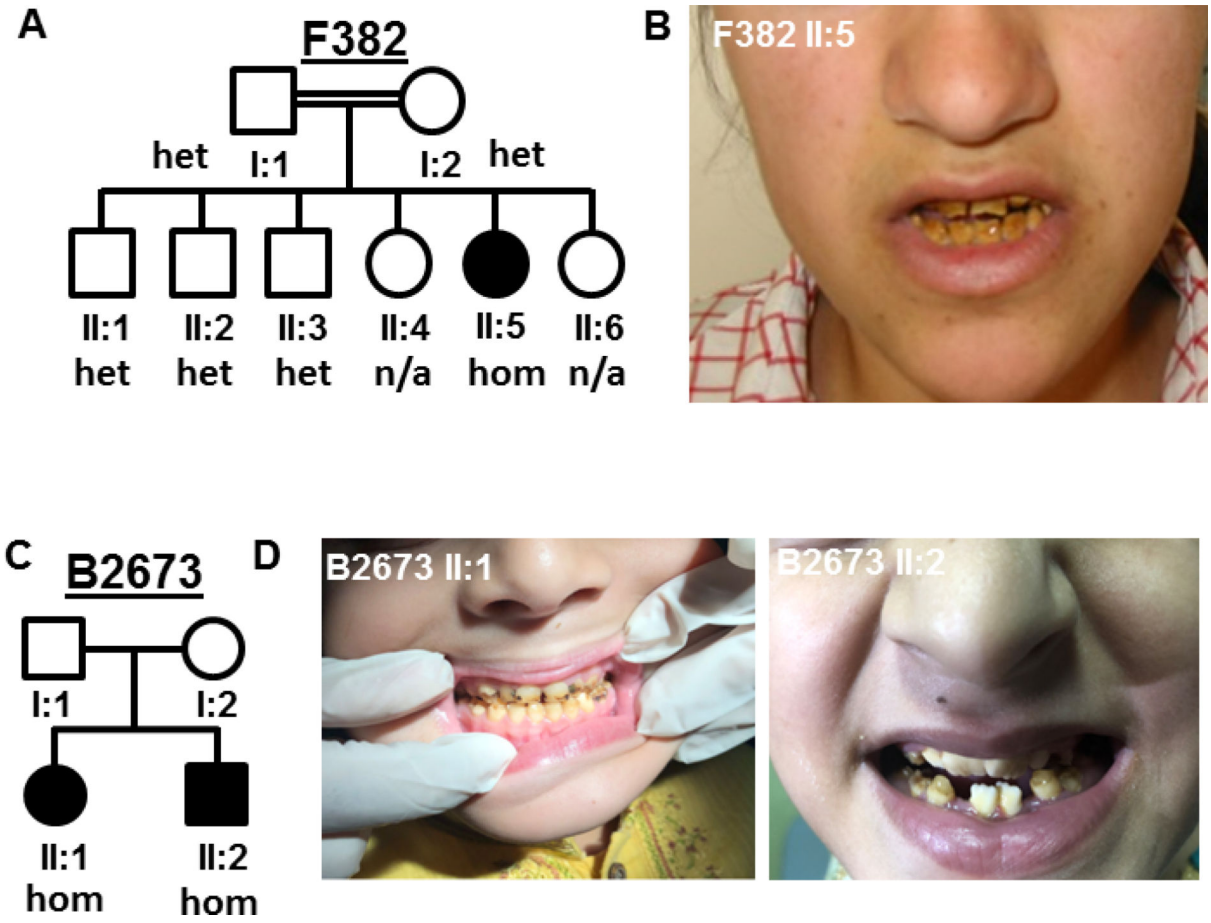

Figure 4: Patients with *WDR72* mutation, dRTA and amelogenesis imperfecta.

Pedigree structure of family F382 (**A**) and B2673 (**C**). (**B, D)** show enamel defects in patient II:5, F382 and patient II:1 and II:2, B2673. het, heterozygous; hom, homozygous.

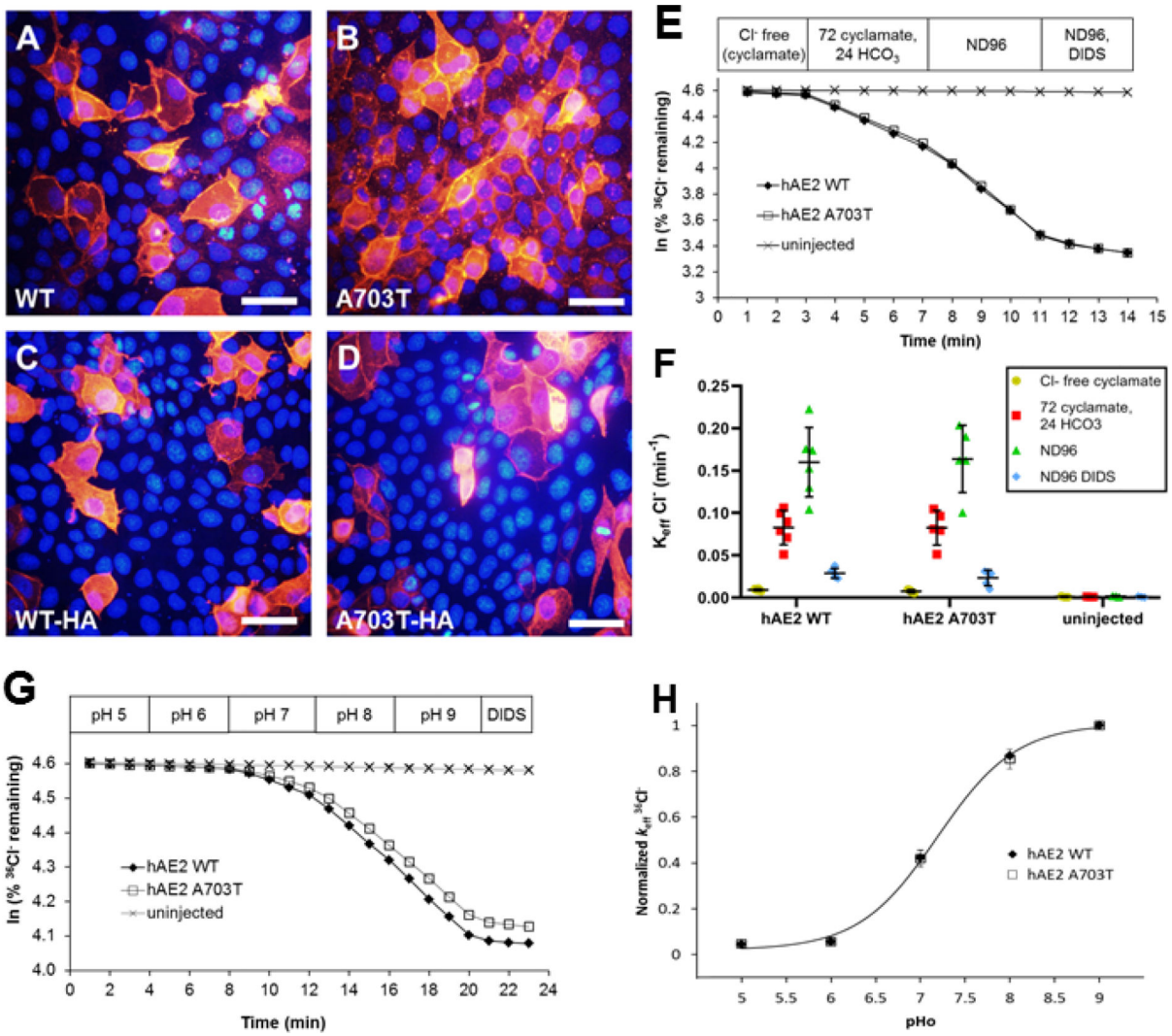

Figure 5. Indistinguishable peripheral membrane localization in MDCK monolayers and indistinguishable rates and regulation by extracellular pH of $^{36}Cl^{-}/HCO_3^{-}$ and $^{36}Cl^{-}/Cl^{-}$ exchange in oocytes expressing hAE2 and hAE2 variant A703T.

(A, B) MDCKII cells plated at high density on glass cover slips were transiently transfected with hAE2 or hAE2 A703T, and immunostained with a rabbit anti-AE2 primary antibody and goat anti-rabbit Cy3-conjugated secondary antibody. Nuclei are DAPI-stained. **(C, D)** Same experiment as in (**A, B)** showing MDCKII cells transiently expressing hAE2-HA or hAE2 A703T-HA, stained with anti-HA primary antibody. Wildtype and variant polypeptides both exhibited prominent peripheral membrane localization. Shown are representative images from one of 3 identical experiments with similar results; scalebars 20 μm. **(E)** $^{36}Cl^{-}$ efflux traces from representative individual oocytes previously injected with 2 ng cRNA encoding hAE2 or hAE2 A703T, or from an uninjected oocyte, during sequential exposure to baths containing nominally impermeant Na cyclamate (96 mM), Na cyclamate (72 mM)/bicarbonate (24 mM), and NaCl (96 mM), followed by final addition of the AE2 inhibitor, DIDS. **(F)** $^{36}Cl^{-}$ efflux rate constants for Cl^{-}/HCO_3^{-} and Cl^{-}/Cl^{-} exchange by oocytes expressing hAE2 (n=6) or variant hAE2 A703T (n=6), compared to uninjected

control oocytes (n=3). Values are means ± S.E.M. **(G)** $^{36}Cl^-$ efflux traces from representative individual oocytes previously injected with 2ng cRNA encoding hAE2 or hAE2 A703T cRNA, or from an uninjected oocyte, during sequential exposure to baths of the indicated increasing pH values. **(H)** Normalized $^{36}Cl^-$ efflux rate constants for oocytes expressing hAE2 and for hAE2 A703T, both fit to a single sigmoidal curve yielding $pH_{o(50)}$ values of 7.19±0.04. Means ± S.E.M. for 5 oocytes in each group.

TABLE 1.

Clinical and genetic data of 10 families with dRTA and mutations in known dRTA genes.

Gene Family - Individual	Nucleotide change	Amino acid change	Exon (zygosity, segregation)	PPH2 score	SIFT	Mut taster	Amino acid conservation to species	Gnomad allele frequencies (hom/ hemi/het/wt)	Mutation reported in Reference	ACMG classification	Gender	Ethnic origin	Parental consanguinity	Age of onset, yrs	Acidosis	Hypokalemia	Urine pH >5.5 under acidosis	Hypercalciuria	Nephro-Calcinosis	Deafness	T reatment
ATP6V0A4, ATPase H+ Transporting V0 Subunit A4 (NM_020632.2)																					
F589 -22	c.2446A>G	p.Lys816Glu	23 (hom, m,p)	0.999	Del	Dis	*S. cerevisiae*	not reported	novel	likely pathogenic	F	Turkey	Yes	2	Yes	Yes	Yes	Yes	Yes	No	$NaHCO_3$, $KHCO_3$
B964 -21	c.1346G>A	p.Arg449His	15 (hom)	1	Del	Dis	*S. cerevisiae*	0/0/3/246,228	62	likely pathogenic	F	n/a	Yes	<1	Yes	Yes	Yes	Yes	Yes	No	K-Citrate, $NaHCO_3$
B1673 -21 -22	c.1312_1315 del	p.Asp438 Metfs*13	14 (hom)	n/a	n/a	n/a	n/a	not reported	63	pathogenic	F F	Serbia Serbia	No No	n/d n/d	Yes Yes	Yes Yes	Yes Yes	Yes Yes	Stones Stones	Yes Yes	K/Na-Citrate, $KHCO_3$
ATP6V1B1, ATPase H+ Transporting V1 Subunit B1 (NM_001692.3)																					
F391 -21	c.1037C>G	p.Pro346Arg	10 (hom, m, p)	1	Del	Dis	*S. cerevisiae*	0/0/4/245,492	4	pathogenic	F	Germany (Turkish)	Yes	<1	Yes	Yes	Yes	n/a	Yes	Yes	$NaHCO_3$, $KHCO_3$
F608 -21	c.497del	p.Thr166 Argfs*9	6 (hom)	n/a	n/a	n/a	n/a	0/0/2/246,220	4	pathogenic	F	Jordan	No	6	Yes	Yes	n/d	n/d	Yes	Yes	$NaHCO_3$, $KHCO_3$
F769 -21	c.242T>C	p.Leu81Pro	3 (hom, m, p)	1	Del	Dis	*S. cerevisiae*	0/0/1/245,488	4	pathogenic	F	Switzerland	No	<1	Yes	n/d	Yes	n/d	Yes	Yes	$NaHCO_3$, K-Citrate
B1459 -21	c.1037C>G	p.Pro346Arg	10 (hom)	1	Del	Dis	*S. cerevisiae*	0/0/4/245,492	4	pathogenic	F	Yemen	No	<1	Yes	Yes	n/d	Yes	Yes	Yes	K-Citrate
SLC4A1, Solute Carrier Family 4 Member 1 (NM_000342.2)																					
F1049 -21	c.1766G>A	p.Arg589His	14 (het)	0.996	Del	Dis	*C. intestinalis*	not reported	5	pathogenic	F	Switzerland (Turkish)	n/a	2	Yes	n/d	Yes	n/d	Yes	No	K/Na-Citrate
B3155 -21	c.2573C>A c.1199_1225del	p.Ala858Asp p.Ala400_Ala408del	19 (het) 11 (het)	0.774 n/a	Del n/a	Dis n/a	*D. melanogaster*	0/0/17/245,910 0/0/13/282,788	64	pathogenic pathogenic	F	Malaysia	Yes	3	Yes	n/d	n/d	n/d	Yes	No	$NaHCO_3$
B2838 -21	c.2573C>A	p.Ala858Asp	19 (hom)	0.774	Del	Dis	*D. melanogaster*	0/0/17/245,910	64	pathogenic	F	Pakistani	Yes	n/d	Yes	No	Yes	Yes	Yes	No	K/Na-Citrate

Del, deleterious; Dis, disease-causing; hemi, hemizygous; het, heterozygous; hom, homozygous; m, maternal; mo., months; n/d, no data; p, paternal; PPH2 score, humvar PolyPhen2 prediction score; SIFT, Sorting intolerant from tolerant; tol, tolerated; VUS, variant of unknown significance; wt, wildtype; yrs, years.

TABLE 2.

Clinical and genetic data of 4 families with dRTA with mutations in the novel candidate genes *ATP6V1C2, WDR72*, and *SLC4A2*.

***Gene* Family - Individual**	**Nucleotide change**	**Amino acid change**	**Exon (zygosity, segregation)**	**PPH2 score**	**SIFT**	**Mut taster**	**Amino acid conservation to species**	**Gnomad allele frequencies (hom/ hemi/het/wt)**	**Mutation reported**	**ACMG classification**	**Gender**	**Ethnic origin**	**Parental consanguinity**	**Age of onset, yrs**	**Acidosis pH HCO_3^- (mmol/L)**	**Hypo-Kalemia (mmol/L)**	**Urine pH >5.5 under acidosis**	**Hypercalciuiria**	**Nephrocalcinosis**	**Deafness**	**Treatment**	**Comment**
ATP6V1C2, ATPase H+ Transporting V1 Subunit C2 (NM_001039362.1)																						
B1022 -21	c.503T>C	p.Ile168Thr	7 (hom, m, p)	0.975	Del	Dis	*C. intestinalis*	0/0/224/277222	novel	likely pathogenic	F	Egypt	Yes	<1	Yes ph 7.2 HCO_3^- 10	Yes 1.8	8.6	No	No	No	Polycitrate Potassium	Death age 9 mo due to renal failure
WDR72, WD Repeat Domain 72 (NM_182758.3)																						
F382 -25	c.477_485dup	p.(Ile159_Cys161dup)	5 (hom)	n/a	n/a	n/a	n/a	not reported	novel	likely pathogenic	F	Turkey	Yes	5	Yes pH 7.1 HCO_3^- 11.5	Yes 2.5	8	Yes	Yes	No	$NaHCO_3$ $KHCO_3$	Enamel Defect
B2673 -21 -22	c.764_768delGGCAG	p.Gly255Val fs*40	8 (hom)	n/a	n/a	n/a	n/a	0/0/1/246104	novel	pathogenic	F M	Indian	No	3 <1	Yes 11 Yes 10	Yes 2.4 Yes 2.8	7 7.5	No No	No No	Yes n/d	$NaHCO_3$ $KHCO_3$	Enamel Defect Enamel Defect
SLC4A2, Solute Carrier Family 4 Member 2 (NM_01199692.2)																						
F588 -21	c.2107G>A	p.Ala703Thr	14 (hom, m, p)	0.995	Del	Dis	*G. gallus*	0/0/1/250904	novel	VUS	F	Turkey	Yes	1	Yes 7.1	Yes 2.5	7	Yes	Yes	Yes	$NaHCO_3$, $KHCO_3$	

Del, deleterious; Dis, disease-causing; hemi, hemizygous; het, heterozygous; hom, homozygous; m, maternal; mo., months; n/d; no data; p, paternal; PPH2 score, humvar PolyPhen2 prediction score; SIFT, Sorting intolerant from tolerant; tol, tolerated; wt, wildtype; yrs, years.